Viscosity Effects on Hydrodynamic Drainage Force Measurements Involving Deformable Bodies

ARTICLE *in* LANGMUIR · JULY 2010

Impact Factor: 4.46 · DOI: 10.1021/la1012473 · Source: PubMed

6 AUTHORS, INCLUDING:

Raymond Riley Dagastine
University of Melbourne
88 PUBLICATIONS **1,633** CITATIONS
SEE PROFILE

Grant B Webber
University of Newcastle
51 PUBLICATIONS **782** CITATIONS
SEE PROFILE

Rogerio Manica
Institute Of High Performance Computing
44 PUBLICATIONS **750** CITATIONS
SEE PROFILE

Derek Y C Chan
University of Melbourne
244 PUBLICATIONS **7,843** CITATIONS
SEE PROFILE

Langmuir Article

pubs.acs.org/Langmuir

Viscosity Effects on Hydrodynamic Drainage Force Measurements Involving Deformable Bodies

Raymond R. Dagastine,*[,†,‡] Grant B. Webber,[†,‡,▽] Rogerio Manica,[⊥] Geoffrey W. Stevens,[†,‡] Franz Grieser,[†,§] and Derek Y. C. Chan[†,∥,#]

[†]*Particulate Fluids Processing Centre,* [‡]*Department of Chemical and Biomolecular Engineering,* [§]*School of Chemistry, and* [∥]*Department of Mathematics and Statistics, University of Melbourne, Parkville, Victoria 3010, Australia,* [⊥]*Institute of High Performance Computing, 1 Fusionopolis Way, #16-16 Connexis, 138632, Singapore, and* [#]*Department of Mathematics, National University of Singapore, 117543, Singapore.* [▽]*Present address: Centre for Advanced Particle Processing, The University of Newcastle, Callaghan, NSW 2308, Australia*

Received March 29, 2010. Revised Manuscript Received May 26, 2010

Dynamic force measurements have been made between an oil drop and a silica particle in surfactant and sucrose solutions with viscosities that range up to 50 times that of water. These conditions provide variations in the shear rate and the relative time scales of droplet deformation and hydrodynamic drainage in a soft matter system. The results obtained indicate that soft deformable boundaries have a natural response that limits the maximum shear rate that can be sustained in thin films compared to shear rates that can be attained in films bounded by rigid boundaries. In addition, to extend boundary slip studies on rigid surfaces, we use a smooth deformable droplet surface to probe the dependence of the boundary slip on fluid viscosity without the added complications of surface roughness or heterogeneity. Imposing a Navier slip model to characterize possible slip at the deformable oil−sucrose solution interface gives results that are consistent with a slip length of no larger than 10 nm over the range of solution viscosity studied, although an immobile (zero slip length) condition at the oil−sucrose solution interface is perfectly adequate. In high viscosity solutions, cantilever motion at high scan rates induces a significant cantilever deflection. A method has been developed to account for this effect in order to extract the correct dynamic force between the deformable drop and the particle.

1. Introduction

The transport of liquids of various viscosities confined near soft surfaces is of increasing interest because of its fundamental relevance in processes as diverse as the motility of biological cells to the formulation and transport of structured emulsions.[1] In microfluidic devices, the use of soft boundaries provides a potential solution for drag reduction to minimize energy expenditures[2] and offers a novel dimension for manipulating localized flow.[3] These types of innovations are seen as crucial for high throughput applications in which the benefits of a quantitative understanding of the hydrodynamic boundary conditions for flow at soft surfaces have not been fully explored.[4] The manipulation of flow properties and boundary conditions in soft matter systems offers a new degree of flow control that may not be possible with rigid boundaries. Furthermore, changes in viscosity affect the response time scales associated with soft material deformations from hydrodynamic perturbations, drag reduction schemes,[2] molecular and interfacial transport,[5−9] and hydrodynamic boundary conditions.[2,4,6]

In quantifying boundary slip using direct force measurements with the atomic force microscope (AFM), sucrose solutions of varying concentrations have been the liquid of choice because they maintain Newtonian liquid behavior over a large range of viscosities.[10−15] At solid surfaces, flow behavior in regimes of high shear rates in which boundary slip effects may be more prominent can be explored by increasing the fluid viscosity. However, at soft boundaries, geometric deformations that arise in response to stresses from the flow field may provide a natural regulating mechanism that limit the range of shear rates that can be attained. As a consequence, boundary slip phenomena that may be observed at rigid boundaries may not be manifested at soft interfaces.

To describe and quantify possible boundary slip at the fluid−solid interface, the Navier slip model postulates that for a Newtonian fluid, the tangential velocity $\mathbf{u}_{\|}$ at the fluid boundary (with unit normal $\mathbf{n}$) is proportional to the local tangential shear stress:[2,16] $\mathbf{u}_{\|} = b\mathbf{n}\cdot[\nabla\mathbf{u} + (\nabla\mathbf{u})^T]\cdot(\mathbf{I} - \mathbf{nn})$. The parameter b, called the slip length, encapsulates details of the interaction between the fluid and the solid boundary. At fluid−solid boundaries, the no-slip or fully immobile boundary condition

*To whom correspondence should be addressed. E-mail: rrd@unimelb.edu.au.

(1) Niu, X. Z.; Zhang, B.; Marszalek, R. T.; Ces, O.; Edel, J. B.; Klug, D. R.; deMello, A. J. *Chem. Commun.* **2009**, 6159–6161.
(2) Rothstein, J. P. *Ann. Rev. Fluid Mech.* **2010**, 42.
(3) Leslie, D. C.; Easley, C. J.; Seker, E.; Karlinsey, J. M.; Utz, M.; Begley, M. R.; Landers, J. P. *Nat. Phys.* **2009**, *5*, 231–235.
(4) Stone, H. A. *Nat. Phys.* **2009**, *5*, 178–179.
(5) Abid, S.; Chesters, A. K. *Int. J. Multiphase Flow* **1994**, *20*, 613–629.
(6) Davis, R. H.; Schonberg, J. A.; Rallison, J. M. *Phys. Fluids A* **1989**, *1*, 77–81.
(7) Edwards, S. A.; Carnie, S. L.; Manor, O.; Chan, D. Y. C. *Langmuir* **2009**, *25*, 3352–3355.
(8) Manor, O.; Vakarelski, I. U.; Stevens, G. W.; Grieser, F.; Dagastine, R. R.; Chan, D. Y. C. *Langmuir* **2008**, *24*, 11533–11543.
(9) Manor, O.; Vakarelski, I. U.; Tang, X.; O'Shea, S. J.; Stevens, G. W.; Grieser, F.; Dagastine, R. R.; Chan, D. Y. C. *Phys. Rev. Lett.* **2008**, *101*, 024501/1–024501/4.
(10) Bonaccurso, E.; Butt, H.-J.; Craig, V. S. J. *Phys. Rev. Lett.* **2003**, *90*, 144501.
(11) Craig, V. S. J.; Neto, C.; Williams, D. R. M. *Phys. Rev. Lett.* **2001**, *87*, 054504.
(12) Henry, C. L.; Craig, V. S. J. *Phys. Chem. Chem. Phys.* **2009**, *11*, 9514–9521.
(13) Honig, C. D. F.; Ducker, W. A. *Phys. Rev. Lett.* **2007**, *98*, 028305/1–028305/4.
(14) Honig, C. D. F.; Ducker, W. A. *J. Phys. Chem. C* **2007**, *111*, 16300–16312.
(15) Neto, C.; Evans, D. R.; Bonaccurso, E.; Butt, H.-J.; Craig, V. S. J. *Rep. Prog. Phys.* **2005**, *68*, 2859–2897.
(16) Lauga, E.; Brenner, M. P.; Stone, H. A. *Springer Handb. Exp. Fluid Mech.* **2007**, *19*, 1219–1240.

corresponds to $b = 0$, while partially mobile interfaces are characterized by a nonzero slip length.

For fluid−fluid interfaces, the effects of changing viscosity at boundaries of simple soft material such as drops and bubbles can be quantified by examining the behavior of the tangential stress across the interface. Across an ideal clean fluid−fluid boundary where the interface is fully mobile, the tangential stress is expected to be continuous across the interface where the velocity of the fluid adjacent to the interface in each phase is moving at the same speed. The presence of mobile surface-active materials at the interface can provide a tangential gradient in the interfacial tension that will give rise to a jump discontinuity in the tangential shear stress.[17] If the gradient of the interfacial tension is sufficiently high, the interface becomes immobile and the hydrodynamic boundary condition at such an interface will be the same as that at a fluid−solid interface that obeys the no-slip condition.

There is often confusion when using the terminology of a "no-slip" boundary condition for a fluid−fluid interface. For a fluid−fluid interface, a fully mobile interface, where the adjacent tangential velocities of the two fluids are equal, satisfies the "no-slip" condition, as the tangential velocities are proportional to the local tangential shear stress for Newtonian fluids. For a fluid−solid interface, when there is a partial or full mobility at the interface, then the tangential velocities are not proportional to the local tangential shear stress (since a solid is not moving, but the fluid is) and there is slip at a surface. In this paper, we describe fluid−fluid interfaces as either mobile or immobile and only use the term "no-slip" to refer to the scenario where the tangential velocity of the fluid−solid or fluid−fluid is zero where in *both* instances the interface is immobile.

In contrast to all previous slip studies with the AFM,[10,11,13,15,18,19] our objective is to use the smooth deformable fluid−fluid interface of a droplet in aqueous solution as a simple model system to examine slip. We quantify flow conditions of fluids with a range of viscosities when they are confined by smooth deformable boundaries. The known deformation characteristics of the fluid−fluid interface and its relative sharpness allow us to make confident estimates of the possible effects of boundary slip at smooth soft surfaces. In particular, it offers a way to quantify boundary slip without complications that may be due to surface roughness,[10] heterogeneities,[20] or effects due to liquid structuring at surfaces.

To quantify dynamic effects of viscosity on force measurements using the AFM, we investigate the time dependent force between a smooth solid silica colloidal probe particle and a smooth deformable oil drop in relative motion in aqueous solutions. The solution viscosity can be varied by a factor of over 50 through varying the sucrose concentration. The quantitative behavior of the dynamic force is determined by the boundary conditions at the solid−sucrose solution and oil−sucrose solution interface that control the flow of the solution in the gap between the particle and the oil drop. However, this gap, of the order of tens of nanometers thick, is large compared to the dimensions of the sucrose molecule (<0.9 nm) so the aqueous solution can still be regarded as a continuum. We use a silica particle probe as one of the interacting surfaces because the hydrodynamic boundary condition on such a hydrophilic surface has now been established unambiguously.[13] All experimental results reported in this paper are taken with the same cantilever and colloidal probe particle.

(17) Levich, V. *Physicochemical Hydrodynamics*; Prentice Hall: London, 1962.
(18) Vinogradova, O. I. *Langmuir* **1996**, *12*, 5963–5968.
(19) Vinogradova, O. I.; Yakubov, G. E. *Phys. Rev. E* **2006**, *73*, 045302/1–045302/4.
(20) Chan, D. Y. C.; Uddin, M. H.; Cho, K. L.; Liaw, I. I.; Lamb, R. N.; Stevens, G. W.; Grieser, F.; Dagastine, R. R. *Faraday Discuss.* **2009**, *143*, 151–168.

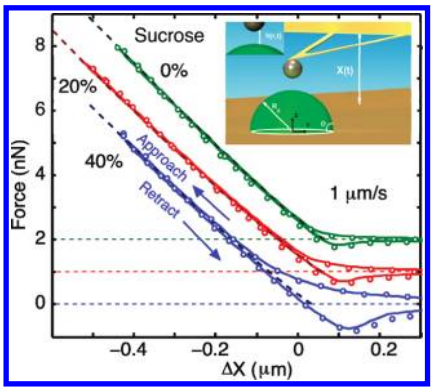

Figure 1. Measured forces (~1% of acquired points are shown) between a silica colloid probe and the tetradecane oil drop in sucrose solution with 5 mM SDS versus relative cantilever displacement, ΔX at a scan rate of 1 μm/s. Experiments are compared to predictions of the Stokes-Reynolds−Young−Laplace model with the immobile boundary condition at the oil drop (− − −) and the analytic high force formula given by eq 8 (---). For clarity, results at different sucrose concentrations have been offset vertically. The upper (lower) data points of each set are the forces on approach (retract). Inset: Schematic diagram of the cantilever with colloid probe and oil drop on the substrate.

2. Experimental Method

In AFM force measurements, a piezoelectric actuator is used to move the end of the cantilever toward or away from the substrate to vary the separation $X(t)$ (Figure 1, inset) between the particle on the cantilever tip and the oil drop on the substrate. The interaction between the particle and the drop will cause the deflection of the cantilever to change as the cantilever is moved. This deflection can be converted to the force between the particle and the drop via Hooke's law, once the cantilever spring constant has been determined. However, in regimes of high scan rates and at high viscosities, the cantilever will also deflect as a result of the hydrodynamic drag exerted on it as it is being driven by the piezoelectric actuator. We have developed a model to characterize cantilever deflections that result from hydrodynamic drag that is separate from deflections due to interaction between the particle and the drop. This is particularly important since the piezoelectric actuator actually moves the cantilever with a variable velocity with the result that such deflections can potentially be misinterpreted as a variable force between the particle and the drop.

An atomic force microscope (Asylum Research, Santa Barbara, CA) was used to measure the dynamic force between a tetradecane oil drop in aqueous sucrose solution with a silica colloid probe particle of radius $R_p = 25 \pm 2$ μm glued on the end of a cantilever (Veeco MLCT Series) whose spring constant, $K = 0.039 \pm 0.004$ N/m, was calibrated by the Hutter−Bechhoefer method.[21] The shear viscosity, μ, of the sucrose solution was varied by up to 50 times that of water by increasing the sucrose concentration to 60%. The sucrose solution also contained 5 mM of the anionic surfactant sodium dodecyl sulfate (SDS), which is below the critical micelle concentration of 8 mM. Force measurements were taken with the probe particle carefully aligned with the apex of the sessile oil drop of undeformed radius $R_d = 107 \pm 2$ μm on the substrate.

A force measurement run comprised an *approach* branch, as the cantilever was moved toward the oil drop by piezoelectric actuator, followed by a *retract* branch, when the cantilever was moved away from the drop. The position, $X(t)$ (Figure 1, inset), of the cantilever was monitored by using a linear variable differential transformer (LVDT). The nominal speed or scan rate of the piezoelectric actuator was varied from less than 1 μm/s up to 20 μm/s. At a set scan rate, the actuator velocity was observed to

(21) Hutter, J. L.; Bechhoefer, J. *Rev. Sci. Instrum.* **1993**, *64*, 1868–1873.

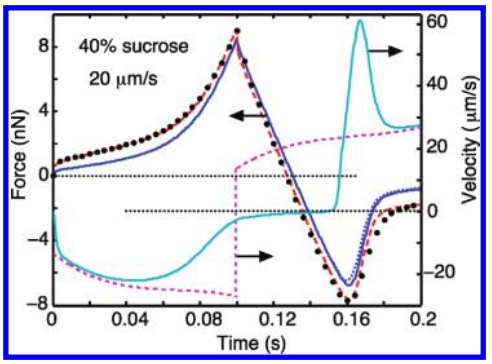

Figure 2. Left axis: Time dependence of the measured (●, ~1% of the acquired data are shown) and predicted (red dashed line) apparent force, $F_{apparent}$, and the predicted interaction force, F, according to the SRYL model with immobile boundary conditions (blue solid line) and with a slip length of 10 nm at the oil−sucrose solution interface (blue dashed line) at a scan rate of 20 μm/s in 40% sucrose solution with 5 mM SDS. Right axis: Piezoelectric drive speed dX/dt (pink dashed line) and central film velocity $dh(0,t)/dt$ (teal solid line).

vary by up to ±50% during the approach and retract runs (see Figure 2), so values of the instantaneous velocity, $dX(t)/dt$, were used in all data analysis and modeling.

Time variations of the cantilever deflection can be converted to the interaction force between the colloidal particle probe and the tetradecane drop. However, at high scan rates and high viscosities, the cantilever also deflects as a result of its motion. Such deflections are additional to that caused by interaction between the particle probe and the drop, and they need to be subtracted from the measured total cantilever deflection in order to derive the dynamic force between the particle and the drop.

The SDS adsorbs onto the surface of the tetradecane drops and creates a negative surface charge.[22] Thus, there was a repulsive electric double layer repulsion between the oil drop and the negative silica particle which was sufficient to prevent particle−oil drop coalescence. The range of the repulsive electrical double layer interaction was not expected to affect the long-ranged hydrodynamic interaction.[23] The adsorbed SDS was also expected to dominiate the influence of low concentrations of adventitious surface active species that generally exist at oil−water interfaces. The surface potential of the silica sphere as a function of sucrose concentration was determined by fitting a electrical double layer model to the sphere-plate AFM force measurements performed using silica spheres from the same batch as the spheres used in the droplet measurements. The tetradecane droplet zeta potential is based on electrokinetic measurements in SDS solutions.[22] These values are not expected to deviate significantly, as the SDS is much more surface active than the sucrose.

Properties of the system and parameters used in analyzing experimental results are given in Table 1. The pendent drop technique was used to measure interfacial tensions with SDS up to 30% sucrose, but the method was not accurate at high viscosities. Therefore, the interfacial tension of the 5 mM SDS and 40% or 60% sucrose was estimated using the high force result in eq 8 (see later). These estimates are also consistent with an extrapolation of a Frumkin isotherm model fit to the lower concentration sucrose−SDS data.

3. Theoretical Analysis

As the particle and drop dimensions are many tens of micrometers whereas interaction between the particle and the oil drop is only significant when their separation is of order tens of nanometers,

Table 1. Properties of the Experimental System and Parameters Used in Modeling at 5 mM SDS and Different Sucrose Concentrations

sucrose (%)	0	20	40	60
interfacial tension, σ (±2 mN/m)	16	8.0	9.0[a]	10[a]
viscosity, μ (Pa s)[24]	0.001	0.0019	0.0058	0.052
silica sphere surface potential (±10 mV)	−40	−25	−25	−25
tetradecane droplet zeta potential[22] (±10 mV)	−100	100	−100	−100
spring constant, K (±0.004 N/m)	0.039			
radius of drop, R_d (±2 μm)	107			
radius of sphere, R_p (±2 μm)	25			
contact angle of drop,[23] θ_o (±5°)	50°			

[a] Derived by fitting using eq 8.

the hydrodynamic problem can be treated in the lubrication approximation.[25] The experimental setup has axial symmetry and can be described by coordinates (r, z) so the time evolution of the separation $h(r,t)$ between the particle and the oil drop (see Figure 1, inset) can be described by the Stokes−Reynolds equation:[26]

$$\frac{\partial h}{\partial t} = \frac{1}{12\mu r}\frac{\partial}{\partial r}\left(r\left[\frac{h^4 + (b_d + b_p)h^3 + 12 b_d b_p h^2}{b_d + b_p + h}\right]\frac{\partial p}{\partial r}\right) \quad (1)$$

where $p(r,t)$ is the hydrodynamic pressure in the sucrose solution between the oil drop and the particle. Whereas this equation allows for different Navier slip lengths at the particle, b_p, and at the oil drop, b_d, we will set $b_p = 0$ since we know that the no-slip condition holds at the particle surface.[13]

The separation between the particle and the oil drop during the course of the dynamic interaction is described by the Young−Laplace equation:[27]

$$\frac{\sigma}{r}\frac{\partial}{\partial r}\left(r\frac{\partial h}{\partial r}\right) = 2\sigma\left(\frac{1}{R_d} + \frac{1}{R_p}\right) - (p + \Pi) \quad (2)$$

where the oil−sucrose solution interfacial tension, σ, is assumed to be constant and the disjoining pressure, $\Pi(r,t)$, accounts for surface forces such as electrical double layer repulsion and van der Waals attraction that are of relatively short-range compared to hydrodynamic interactions. Equations 1 and 2 are both referred to as the Stokes−Reynolds−Young−Laplace (SRYL) equations, which together with appropriate initial and boundary conditions can be solved by the method of lines[25,28] from which the dynamic force, $F(t)$, between the particle and the oil drop can be calculated:

$$F(t) = 2\pi\int_0^\infty r[p(r,t) + \Pi(r,t)]dr \quad (3)$$

Axial symmetry considerations require the spatial derivative of the pressure and the separation to be zero at $r = 0$: $\partial p/\partial r = 0 = \partial h/\partial r$. In the lubrication limit, the initial separation between the particle and the undeformed drop has the parabolic form,

$$h(r, t = 0) = h_o + r^2/R_o, \quad R_o{}^{-1} \equiv \left(R_p{}^{-1} + R_d{}^{-1}\right) \quad (4)$$

(22) Nespolo, S. A.; Bevan, M. A.; Chan, D. Y. C.; Grieser, F.; Stevens, G. W. *Langmuir* **2001**, *17*, 7210–7218.
(23) Webber, G. B.; Manica, R.; Edwards, S. A.; Carnie, S. L.; Stevens, G. W.; Grieser, F.; Dagastine, R. R.; Chan, D. Y. C. *J. Phys. Chem. C* **2008**, *112*, 567–574.
(24) Green, D. W.; Perry, R. H. *Perry's Chemical Engineering Handbook*; McGraw-Hill: New York, 2008.
(25) Carnie, S. L.; Chan, D. Y. C.; Lewis, C.; Manica, R.; Dagastine, R. R. *Langmuir* **2005**, *21*, 2912–2922.
(26) Manica, R.; Connor, J. N.; Carnie, S. L.; Horn, R. G.; Chan, D. Y. C. *Langmuir* **2007**, *23*, 626–637.
(27) Manica, R.; Connor, J. N.; Dagastine, R. R.; Carnie, S. L.; Horn, R. G.; Chan, D. Y. C. *Phys. Fluids* **2008**, *20*, 032101/1–032101/12.
(28) Dagastine, R. R.; Manica, R.; Carnie, S. L.; Chan, D. Y. C.; Stevens, G. W.; Grieser, F. *Science* **2006**, *313*, 210–213.

The initial distance of closest approach, h_o, between the particle and the drop can be set experimentally to be in the range of 1−6 μm in a force run. Its precise value can be determined to within ±0.01 μm by requiring the model to fit the entire force curve. Far from the central axis, where $r \rightarrow \infty$, the pressure vanishes as $p \sim r^{-4}$ and this condition is implemented as[27] $r(\partial p/\partial r) + 4p = 0$.

For measurements in low viscosity liquids, the dynamic force, F, between the particle and the drop is obtained from the measured cantilever deflection, S, and the cantilever spring constant, K, by applying Hooke's law: $F = KS$. However, at high scan rates and in high viscosity solutions, the cantilever also deflects due to hydrodynamic drag when it is being moved by the piezoelectric actuator. We expect that, under Stokes flow, this deflection, S_{drag}, will be proportional to the actuator velocity, dX/dt, and the viscosity, μ, of the solution and inversely proportional to the cantilever spring constant, K:

$$S_{drag} = -C\frac{\mu}{K}\frac{dX}{dt} \tag{5}$$

The sign convention in eq 5 is such that a positive deflection corresponds to an apparent repulsion between the particle and the drop. The constant, C, can be determined from the force curve at large separations when drop deformation is negligible and its value will depend only on the geometric properties of the cantilever.

Following earlier work,[25,28−33] we use the constant volume constraint to obtain the following boundary condition at the outer limit of the solution domain, $r = r_{max}$, if the three phase contact line of drop on the substrate is assumed to be immobile:

$$\frac{\partial h}{\partial t} = \frac{dX}{dt} - C\frac{\mu}{K}\frac{d^2X}{dt^2} + \frac{1}{K}\left(\frac{dF}{dt}\right) - \frac{1}{2\pi\sigma}\left(\frac{dF}{dt}\right)\left[1 + \frac{1}{2}\log\left(\frac{{r_{max}}^2}{4{R_d}^2}\right) + \frac{1}{2}\log\left(\frac{1+\cos\theta_o}{1-\cos\theta_o}\right)\right] \tag{6}$$

Here, θ_o is the contact angle of the undeformed drop on the substrate. On the other hand, if the drop on the substrate maintains a constant contact angle, θ, this boundary condition would be

$$\frac{\partial h}{\partial t} = \frac{dX}{dt} - C\frac{\mu}{K}\frac{d^2X}{dt^2} + \frac{1}{K}\left(\frac{dF}{dt}\right) - \frac{1}{2\pi\sigma}\left(\frac{dF}{dt}\right)\left[1 + \frac{1}{2}\log\left(\frac{{r_{max}}^2}{4{R_d}^2}\right) + \frac{1}{2}\log\left(\frac{1+\cos\theta}{1-\cos\theta}\right) - \frac{1}{2+\cos\theta}\right] \tag{7}$$

The derivations of eqs 6 and 7 are given in the Appendix. However, we should note that cantilever drag also affects the form of the large r boundary condition, eq 6 or 7, for the SRYL equations that determine the dynamic interaction between the particle and the deformable drop.

At low scan rates and in the regime when the repulsive force between the particle and the drop is high so that the approach and retract force data overlap, the force, F, versus relative cantilever displacement, ΔX (up to an additive constant), has the following approximate analytic form[27]

$$\Delta X \sim \frac{F}{4\pi\sigma}\left[\log\left(\frac{FR_o}{8\pi\sigma{R_d}^2}\right) + \log\left(\frac{1+\cos\theta_o}{1-\cos\theta_o}\right) + 1\right] \tag{8}$$

This result is independent of viscosity or details of the disjoining pressure as long as it is sufficiently repulsive to prevent coalescence. It provides a useful check between theory and experiment. Furthermore, the interfacial tension, σ, of the drop determined from this result can be compared to values that have been measured independently.[23,34]

4. Results and Discussion

Low Scan Rates, Variable Viscosity. Results for the force, F, versus relative cantilever position, ΔX, at a low scan rate (1 μm/s) are shown in Figure 1 for 0%, 20%, and 40% aqueous sucrose solutions, where, for clarity, only about 1% of measured data points have been plotted. At this low scan rate, cantilever deflection due to hydrodynamic drag is negligible. However, the almost 6-fold increase in solution viscosity over this sucrose concentration range enhances the hydrodynamic interaction and gives rise to the growth of the size of the hysteresis loop between the approach and retract branches of the force. At these low scan rates, the SRYL model gives excellent agreement between theory and experiments, particularly with regards to the region around the force hysteresis using the no-slip and immobile hydrodynamic boundary condition, corresponding zero slip lengths: $b_d = 0 = b_p$, at the particle and at the deformable tetradecane drop. Earlier AFM studies[9,23,28,34,35] examining the presence of Marangoni flows, electrokinetic measurements,[22,35,36] or larger scale drainage studies studies[37,38] have shown that a very low concentration of surfactant is sufficient to give rise to an immobile interface. In this work, at the concentration of 5 mM SDS in the sucrose solution, which is below the CMC value of 8 mM, the surface coverage is around 90% saturation[22] and thus an immobile interface is expected for this oil and surfactant system.

In the high force region (>2 nN) where the approach and retract data overlap, the force, F, as a function of displacement, ΔX, dependence can be fitted to the high force analytic result (dashed lines) given in eq 8.[26,27] The fitting procedure also allows the interfacial tension of the tetradecane drop at various sucrose concentrations to be determined (Table 1). The interfacial tensions obtained this way agreed with available values determined by the pendent drop method. This high force analytic result does not depend on the detailed form of the repulsive disjoining pressure, $\Pi(r,t)$, as long as the particle and the drop are prevented from coalescing.

High Scan Rates, Variable Viscosity. At higher scan rates, and particularly at high solution viscosities, it is important to quantify separate contributions to the observed deflection, S, of the cantilever due to interaction between the particle and the drop and due to hydrodynamic drag on the cantilever. Significant cantilever deflection due to hydrodynamic drag is evident even

(29) Bardos, D. C. *Surf. Sci.* **2002**, *517*, 157–176.
(30) Chan, D. Y. C.; Dagastine, R. R.; White, L. R. *J. Colloid Interface Sci.* **2001**, *236*, 141–154.
(31) Dagastine, R. R.; White, L. R. *J. Colloid Interface Sci.* **2002**, *247*, 310–320.
(32) Nespolo, S. A.; Chan, D. Y. C.; Grieser, F.; Hartley, P. G.; Stevens, G. W. *Langmuir* **2003**, *19*, 2124–2133.
(33) Dagastine, R. R.; Prieve, D. C.; White, L. R. *J. Colloid Interface Sci.* **2004**, *269*, 84–96.
(34) Webber, G. B.; Edwards, S. A.; Stevens, G. W.; Grieser, F.; Dagastine, R. R.; Chan, D. Y. C. *Soft Matter* **2008**, *4*, 1270–1278.
(35) Aston, D. E.; Berg, J. C. *Ind. Eng. Chem. Res.* **2002**, *41*, 389–396.
(36) Baygents, J. C.; Saville, D. A. *J. Chem. Soc., Faraday Trans.* **1991**, *87*, 1883–1898.
(37) Klaseboer, E.; Chevaillier, J. P.; Gourdon, C.; Masbernat, O. *J. Colloid Interface Sci.* **2000**, *229*, 274–285.
(38) Neumann, B.; Vincent, B.; Krustev, R.; Muller, H. J. *Langmuir* **2004**, *20*, 4336–4344.

when the colloid probe is far from the oil drop, particularly at high viscosities. Hitherto, this drag force has been assumed to be constant and its value is estimated by using an additive constant to enforce a zero force at large separations.[13,39] However, linearity of the hydrodynamic problem suggests that the cantilever drag force should be proportional to the velocity of the cantilever and the solution viscosity. In section 3, we indicate that cantilever drag has to be taken into account in formulating an appropriate boundary condition for the SRYL model.

We can define the measured apparent force, $F_{apparent}$, as the product of the observed cantilever deflection, S, and the cantilever spring constant, K. This can be written as the sum of a separation-independent cantilever drag force, F_{drag}, and the interaction force, F:

$$F_{apparent} \equiv KS = F_{drag} + F = -KS_{drag} + F = C\mu\, dX(t)/dt + F \quad (9)$$

We determine the value of the constant $C = (6.0 \pm 0.6) \times 10^{-3}$ m for our cantilever, from experimental results in a 40% sucrose solution at 20 μm/s during $0 < t \leq 0.04$ s (Figure 2) when the particle is far from the oil drop and deformation is negligible. In this regime, the analytical form of $F = -(6\pi\mu R_o^2/h)(dX/dt)$ (without deformations) can be used. The value of C so obtained is then used to analyze all other data obtained with the same cantilever at different scan rates and different viscosities.

In Figure 2, we compare experimental apparent force data, $F_{apparent}$, in a 40% sucrose (with 5 mM SDS) solution at 20 μm/s predicted using the solution of the SRYL model given in eqs 1−6. We see excellent quantitative agreement with the no-slip boundary condition at the oil−water interface. From this comparison, we can extract the interaction force, F, between the particle and the deformable drop. The effects of the cantilever drag are significant in regimes where the film drainage velocity is high, as measured by the rate of change of the central film thickness, $dh(0,t)/dt$. From Figure 2, the film drainage rates are high near the rise of the repulsive region during the approach phase and near the hydrodynamic attractive minimum during the retract phase. The effect of using a Navier slip model at the oil−sucrose solution interface with a slip length of 10 nm on the interaction force, F, is also shown in Figure 2. Although the level of precision of the experimental results can accommodate a slip length between 0 and 10 nm, we have no other compelling reason to conclude that slip occurs in our system.

In Figure 3, we compare experimental apparent force data, $F_{apparent}$, and predictions from the SRYL model at the scan rate of 20 μm/s for three different sucrose concentrations that span a 6-fold change in the viscosity. Similar comparisons at lower scan rates show equally good agreement between experiment and theory, again with the immobile boundary condition on the oil drop.

The shear rate at the oil−sucrose solution interface at different radial positions in the film of sucrose solution between the particle and the oil drop is shown in the inset of Figure 3 corresponding to different times marked on the force curve during particle−drop interaction in a 40% sucrose solution. The sign of the shear rate depends on whether the sucrose solution is being expelled from between the oil drop and particle during the approach phase or being sucked in to fill the space between the oil drop and the particle during the retraction phase. The magnitude of the shear rate remains at less than 6200 s^{-1}. The reason for the modest magnitude of shear rate is that the deformability of the oil drop provides a natural limiting mechanism. As the particle is driven toward the drop, the repulsive hydrodynamic pressure will

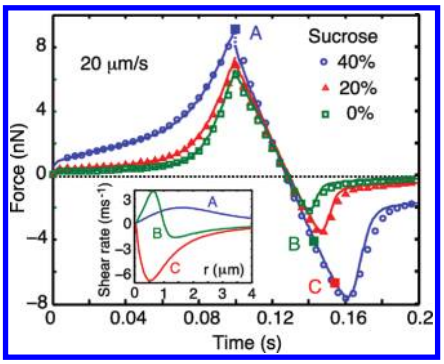

Figure 3. Time dependence of the experimental apparent force, $F_{apparent}$ (points), at three different sucrose concentrations (in 5 mM SDS) and at a scan rate of 20 μm/s. Comparison with the SRYL model with immobile boundary conditions at the oil−sucrose solution interface (lines). Inset: Shear rate at the oil−sucrose solution interface at 40% sucrose as a function of the radial coordinate, r, corresponding to times keyed to the force curve in the main figure.

increase. When this pressure approaches the Laplace pressure of the drop, the oil−sucrose solution interface will begin to deform and flatten, and thereby increase the effective interaction area between the particle and the flattened drop. This enhanced hydrodynamic repulsion is sufficient to prevent the particle from further approaching the oil−water interface. We can see this from the calculated rate of change of the central separation at $r = 0$: $dh(0,t)/dt$, between the drop and the particle shown in Figure 2 (continuous line, right ordinate). During the period $0.10 \text{ s} < t < 0.16$ s, $dh(0,t)/dt$ is small so the separation between the particle and the drop is nearly constant while the force changes significantly in both magnitude and sign. These changes are accompanied by changes in the flow direction of the intervening sucrose solution as reflected in the change in sign of the shear rate (Figure 3, inset).

Interestingly, after the force reaches the attractive minimum during the retraction phase at $t \geq 0.16$ s in Figure 2, the surface of the oil drop separates very quickly from the particle and attains a local speed of ~60 μm/s, almost twice that of the speed of the piezoelectric actuator. At the corresponding force minimum in Figure 3, point C, the shear rate has the largest magnitude (Figure 3, inset).

Highest Solution Viscosity. At the highest sucrose concentration of 60% (Figure 4) where the solution viscosity is over 50 times that of water, we can only drive the cantilever at a maximum speed of 3 μm/s as we need to keep the cantilever response within the linear regime. To demonstrate the effects of incorporating a nonzero slip length at the oil−sucrose solution interface, we also show calculated values of the interaction force that include slip lengths of 10, 100, and 1000 nm at the oil−sucrose solution interface in Figure 4. From this, we conclude that if we wish to allow for the possibility of a nonzero slip length at the deformable tetradecane−sucrose solution interface, a slip length of 10 nm would be an upper bound. Indeed, the present comparison between theory and experiment does not provide compelling evidence of a nonzero slip length. Similar comparisons at other sucrose concentrations lead to the same conclusion (see also Figure 3).

Additional Observations. From the results in Figures 2−4, we note the following:

(i) For times $t \geq 0.7$ s, which is just after the force maximum at point A in Figure 4, the retraction phase has commenced and the particle is being pulled away from the oil drop by the piezoelectric actuator. Nevertheless, we see in the inset of Figure 4 that because the oil drop is deformable, the sucrose

(39) Craig, V. S. J.; Neto, C. *Langmuir* **2001**, *17*, 6018–6022.

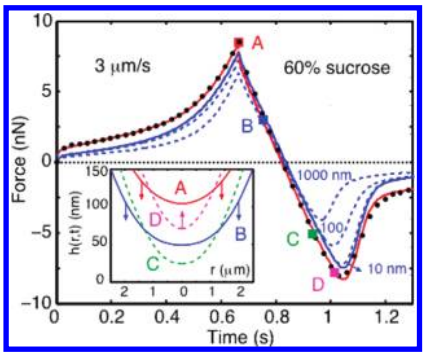

Figure 4. Time dependence of the experimental apparent force, $F_{apparent}$ (●), the interaction force, F, from the SRYL model with no-slip boundary conditions (blue solid line) and with slip lengths ranging between 10 to 1000 nm at the oil−sucrose solution interface (blue dashed line). Inset: Separation between the deformable oil−sucrose solution interface and the particle as a function of the radial coordinate, r, corresponding to times keyed to the force curve in the main figure.

solution film between the particle and the oil drop continues to thin until point C ($t \sim 0.9$ s) where the sucrose film reaches a minimum thickness of around $h \sim 25$ nm (curve C inset Figure 4).

(ii) As the sucrose solution is over 70 nm thick around point D (Figure 4), the physical origin of the force minimum is therefore due entirely to hydrodynamic interactions across a film of sucrose solution confined between the silica particle and the deformed surface of the oil drop. Repulsive electrical double layer interactions and attractive van der Waals forces are negligible at such separations. For such thick films (compared to the size of the sucrose molecule, ~0.9 nm), the sucrose solution can certainly be treated as a continuum Newtonian fluid characterized by a constant shear viscosity.

(iii) In allowing for a slip length of up to 10 nm at the deformable oil−sucrose solution interface, the discernible difference with the immobile interface result occurs at around the force minimum, point C in Figure 3 and point D in Figure 4. The shear rate in the film at these points is large (Figure 3, inset) because the deformable oil−sucrose solution interface is receding rapidly from the particle (Figure 2, for $dh(0,t)/dt$, continuous curve, right ordinate). Thus, with the added degree of freedom of deformability, we see that the effects of boundary slip is most noticeable at high shear rates, which does not necessarily occur when the film thickness is at a minimum as expected for flow between rigid boundaries. The highest shear rate therefore occurs at a point controlled by a combination surface deformability, effective area of interaction, surface separation, and interfacial velocity.

(iv) The detailed analyses developed here for the hydrodynamic drag on the cantilever have up to a 15% effect on measurements at higher viscosities and velocities. It is interesting to note that most slip studies using an AFM on rigid surfaces have not considered accounting for the deflection of the cantilever in this fashion, even though recent studies that examine slip between hydrophilic surfaces report anomalous differences between different types of cantilevers[12] with no definitive explanations, but where the characteristic drag on the cantilever may differ.

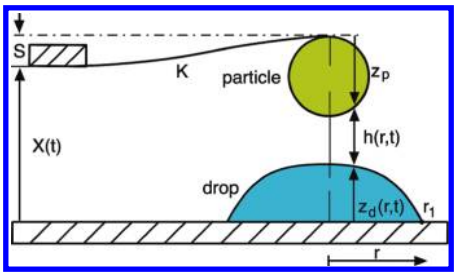

Figure 5. Schematic diagram of the particle-drop geometry in the atomic force microscope.

(v) The use of a Navier slip model at the surface of the oil drop involves a further simplification. If there are mobile surfactants at the oil−sucrose solution interface, one should take into account hydrodynamic flow both in the sucrose solution in between the oil drop and the particle as well as in the interior of the oil drop. These two flow fields will be coupled at the interface by a tangential stress balance condition that involves local tangential gradients of the interfacial tension and convection and diffusion of the mobile surfactants.[6,9] Whereas the formulation of such a detailed model is available, the additional technical complexity involved in implementing this model is quite significant.[7] The present study using the simpler Navier slip model does not provide compelling evidence for a slip length larger than 10 nm, or about 10 times the dimensions of the sucrose molecule. Indeed, a zero slip length is still able to describe the experimental results very well. In addition, mobility of the surface is unlikely given we have approximately 90% saturation of the oil−sucrose solution interface with surfactant. In a noncreeping flow regime, where higher shear rates may be possible, interface mobility may become a more important factor.

5. Conclusions

Using a well-characterized system of an oil drop in a sucrose solution as a model soft smooth interface for which the dynamic behavior is dominated by hydrodynamic interactions, we are able to demonstrate that boundary slip can manifest as a Navier slip length of no more than 10 nm or about 10 times the molecular size of the sucrose molecule under the combined effects of interfacial deformations and a 50-fold variation in solvent viscosity. This is a reasonable expectation since the slip length should reflect characteristic length scales at the fluid interface. The ability of the oil drop to deform suggests that soft systems provide a natural mechanism to limit shear, which will have implications in the possibility of using soft material to minimize energy requirements in massively parallel microfluidic operations.

Acknowledgment. This work is supported in part by the Australian Research Council (ARC) Discovery Grant Scheme and together with AMIRA International and the State Governments of Victoria and South Australia through the ARC Linkage grant scheme. D.Y.C.C. is an Adjunct Professor at the National University of Singapore.

Appendix

The total deflection, S, of the cantilever is caused by fluid drag arising from cantilever motion (dX/dt) and by the interaction

force, F, between a particle and drop. The fluid drag contribution to the deflection, S_{drag}, will be proportional to the piezoelectric actuator velocity, dX/dt, and the viscosity, μ, of the solution and inversely proportional to the cantilever spring constant, K:

$$S = S_{drag} + F/K = -C(\mu/K)(dX/dt) + F/K \quad \text{(A1)}$$

where $S > 0$ corresponds to repulsion and the constant C depends on the cantilever geometry.

From the geometry of schematic atomic force microscope in Figure 5, we have

$$X + S = z_p + h + z_d \quad \text{(A2)}$$

Differentiation with respect to t and noting that particle shape, z_p, is constant gives

$$\begin{aligned} dh/dt &= dX/dt + dS/dt - 0 - dz_d/dt \\ &= dX/dt - C(\mu/K)(d^2X/dt^2) + (1/K)(dF/dt) - dz_d/dt \end{aligned} \quad \text{(A3)}$$

If the three phase contact line of the drop on the substrate is pinned at a constant position during interaction, then at a position $r = r_{max}$ that is outside the interaction zone the drop shape has the form given by eq 21 of Carnie et al.[25]

$$\frac{dz_d}{dt} = \frac{1}{2\pi\sigma}\left(\frac{dF}{dt}\right)\left[1 + \frac{1}{2}\log\left(\frac{r_{max}^2}{4R_d^2}\right) + \frac{1}{2}\log\left(\frac{1+\cos\theta_o}{1-\cos\theta_o}\right)\right] \quad \text{(A4)}$$

where θ_o is the contact angle of the undeformed drop on the substrate. Thus, the boundary condition at $r = r_{max}$, with cantilever drag with the pinned contact line boundary condition, is

$$\begin{aligned} \frac{\partial h}{\partial t} &= \frac{dX}{dt} - C\frac{\mu}{K}\frac{d^2X}{dt^2} + \frac{1}{K}\left(\frac{dF}{dt}\right) \\ &- \frac{1}{2\pi\sigma}\left(\frac{dF}{dt}\right)\left[1 + \frac{1}{2}\log\left(\frac{r_{max}^2}{4R_d^2}\right) + \frac{1}{2}\log\left(\frac{1+\cos\theta_o}{1-\cos\theta_o}\right)\right] \end{aligned} \quad \text{(A5)}$$

On the other hand, if the contact angle the drop on the substrate is constant during interaction, the boundary condition at $r = r_{max}$ can be deduced from eq 25 of Carnie et al.[25] to be

$$\begin{aligned} \frac{dh}{dt} &= \frac{dX}{dt} - C\frac{\mu}{K}\frac{d^2X}{dt^2} + \frac{1}{K}\left(\frac{dF}{dt}\right) \\ &- \frac{1}{2\pi\sigma}\left(\frac{dF}{dt}\right)\left[1 + \frac{1}{2}\log\left(\frac{r_{max}^2}{4R^2}\right) + \frac{1}{2}\log\left(\frac{1+\cos\theta}{1-\cos\theta}\right) - \frac{1}{2+\cos\theta}\right] \end{aligned} \quad \text{(A6)}$$

The relative magnitude of the new term involving (d^2X/dt^2) term in eqs A5 and A6 can be estimated by the standard scaling used in this problem in terms of the capillary number: $Ca = \mu V/\sigma$, where V is the scan rate

$$h \sim R_o Ca^{1/2};\ t \sim (R_o Ca^{1/2})/V;$$

$$r \sim R_o Ca^{1/4};\ F \sim (\sigma/R_o)(R_o Ca^{1/4})^2$$

With this scaling, the various terms in eq A5 have the order:

$$\frac{dh}{dt} \sim \frac{dX}{dt} \sim \frac{1}{2\pi\sigma}\left(\frac{dF}{dt}\right)\left[1 + \frac{1}{2}\log\left(\frac{r_{max}^2}{4R_d^2}\right) + \frac{1}{2}\log\left(\frac{1+\cos\theta_o}{1-\cos\theta_o}\right)\right] \sim O(1)$$

$$\frac{1}{K}\left(\frac{dF}{dt}\right) \sim O(\sigma/K)$$

$$C\frac{\mu}{K}\frac{d^2X}{dt^2} \sim O(C/R)(\sigma/K)Ca^{1/2}$$

Using the estimated value of $C \sim 6 \times 10^{-3}$ m from experimental data and using upper bound estimates for $\mu \sim 5 \times 10^{-3}$ Pa s and $V \sim 20 \times 10^{-6}$ m/s and system parameters $R \sim 50 \times 10^{-6}$ m and system parameters $\sigma \sim 50 \times 10^{-3}$ N/m, $K \sim 40 \times 10^{-3}$ N/n, we find

$$C\frac{\mu}{K}\frac{d^2X}{dt^2} \sim O(C/R)(\sigma/K)Ca^{1/2} \sim 0.14$$

which is around a 14% effect, assuming the scaled (d^2X/dt^2) is of order 1. The effect of this cantilever drag term will be smaller at lower viscosities or scan rates.

In implementing this cantilever drag contribution to the boundary condition at r_{max}, we use the cantilever displacement function, $X(t)$, measured by the LVDT in the AFM. This function, available as a list of data points, exhibits a sharp jump in the value of $dX(t)/dt$ at the commencement of the retract phase. As a result, the value of $d^2X(t)/dt^2$ has an apparent jump discontinuity which is simply an artifact of the discrete nature of data trace of $X(t)$. This then results in a small jump discontinuity in the predicted value of the apparent force just after the commencement of the retraction phase. This technical deficiency can be corrected if finer sampling of the displacement function, $X(t)$, is available.